environments

Article

Environmental Temperature Effect on Hydraulic Behavior and Stability of Shallow Slopes

Shu-Rong Yang [1], Rui-En Chang [2], Ya-Sin Yang [2] and Hsin-Fu Yeh [2,*]

1 Department of Civil Engineering, National Pingtung University of Science and Technology, Pingtung 912, Taiwan; sryang@mail.npust.edu.tw
2 Department of Resources Engineering, National Cheng Kung University, Tainan 701, Taiwan; n46101024@ncku.edu.tw (R.-E.C.); n48061026@ncku.edu.tw (Y.-S.Y.)
* Correspondence: hfyeh@mail.ncku.edu.tw; Tel.: +886-6-275-7575 (ext. 62838)

Abstract: This study established a study framework to quantify the safety factors of unsaturated shallow slopes at different temperatures. This study is based on a non-isothermal soil water characteristic curve model quantifying the temperature-dependent hydraulic properties of soils. The hydraulic coupling analysis models HYDRUS 2D and The Slope Cube Module were used for finite element modeling. A slope stability analysis was performed based on the local factor of safety (LFS) theory. An increased temperature decreased the soil matric suction, suction stress, effective stress, and LFS, weakening the soil strength. Slope modeling analysis showed that soils were dominated by different water retention mechanisms before and after rainfall infiltration, and the trends caused by temperature changes also changed accordingly. This study provides insights into the relationship between soil mechanical properties and temperature, which is valuable for maintaining soil stability and preventing geological hazards.

Keywords: temperature; soil water characteristic curves; hydro-mechanical coupling; slope stability; local factor of safety

Citation: Yang, S.-R.; Chang, R.-E.; Yang, Y.-S.; Yeh, H.-F. Environmental Temperature Effect on Hydraulic Behavior and Stability of Shallow Slopes. *Environments* **2023**, *10*, 134. https://doi.org/10.3390/environments10080134

Academic Editor: Guobin Fu

Received: 23 June 2023
Revised: 24 July 2023
Accepted: 28 July 2023
Published: 1 August 2023

1. Introduction

Global temperatures have increased in recent decades, leading to rapid climate change and increasing the frequency and intensity of natural disasters worldwide, especially rainfall-induced landslides related to climate change [1,2]. The intensity of these disasters is closely linked to unsustainable human development, including climate change, urbanization, globalization, and political and economic instability [3,4]. Observations from the Global Precipitation Climate Center (GPCC) showed an increasing trend in the frequency, duration, and intensity of droughts in different regions of the world from 1951 to 2010. Historical records and future projections suggest that the severity and frequency of heat waves, droughts, and simultaneous droughts are increasing in certain areas [5,6]. These results suggest the need to study the effects of temperature increases on slope stability under climate change scenarios [7,8].

The soil water characteristic curve (SWCC) plays a crucial role in effectively analyzing variations in soil hydraulic properties affected by environmental temperature changes. The SWCC is mainly used to describe the relationship between the matric suction and water content, which is a key factor in studying the behavior of unsaturated soils [9,10]. As rainfall infiltrates unsaturated slopes, the increase in soil water content leads to a loss of matric suction, decreasing the shear strength of the soil and the safety factor of the slope, leading to landslides, debris flows, and other disasters. SWCC is concerned with inherent soil properties, such as texture and structure, as well as soil temperature [11,12]. Variations in soil temperature and water content can induce hazards in water engineering projects, such as frozen soil, embankment collapse, and structural cracking [13]. Therefore, studying the effects of environmental temperature changes on the SWCC of unsaturated soils is of theoretical and engineering significance. Heat and water transfer processes between the ground and atmosphere, as well as through the soil surface, strongly influence the behavior of the unsaturated zone [14,15]. To improve the understanding of slope stability, it is necessary to integrate the parameters affecting the water content and suction of unsaturated soil. The accuracy of the fitting parameters significantly impacts the geotechnical engineering analysis [16]. The effect of temperature on water retention behavior has been studied, and the common conclusion is that water retention capacity decreases with increasing temperature [17]. In most studies, this temperature effect has been attributed to the thermal response of the capillary water in the soil, i.e., a decrease in the surface tension of water, a decrease in the contact angle between the water and the surface of soil particles, and an increase in pore air [18–21]. For the slope stability analysis of temperature change, in recent years, some scholars have evaluated the factor of safety (FOS) of slopes based on the non-isothermal soil water retention curve model [8] and using the limit equilibrium method [22].

Taiwan is located in East Asia and belongs to a subtropical monsoon climate zone. Owing to Taiwan's complex geological conditions and frequent earthquakes, landslides occur more frequently, and the areas affected by landslides caused by extreme rainfall are larger in Taiwan than those affected by large-scale earthquakes worldwide [23], highlighting the need for research on the problem of rain-induced landslides in Taiwan. According to climate change studies, the intensity and frequency of typhoons and extreme rainfall events in Taiwan tend to increase under the influence of extreme weather events and global warming [24–26]. However, research on the effects of temperature on slope stability in Taiwan is lacking. The climate in Taiwan has significant variations and a large day–night temperature difference. Taiwan's densely populated urban areas also suffer from significant urban heat island effects. Studies have indicated an increasing trend in both the average and extreme temperatures in Taiwan [27–29]. Considering the unique geological environment of Taiwan and the need to address its variable climate, it is particularly important to evaluate the influence of temperature variation on shallow slopes. This study evaluated the effects of environmental temperature changes on the hydraulic behaviors and stabilities of shallow slopes. By combining the thermal effect on soil water retention mechanisms and fitting a temperature-dependent SWCC, this study conducted seepage and stress analyses to evaluate the hydraulic behavior of soils under the influence of temperature. Finally, slope stability analysis was performed to further analyze the stability of the slopes. Evaluating variations in the soil hydraulic properties of shallow slopes in reaction to environmental temperature changes is important and can conduce to a better understanding of soil and water conservation and sustainable slope protection in Taiwan.

2. Materials and Methods

2.1. Temperature Dependence of Matric Suction

In this study, the soil water characteristic curve (SWCC) equation considered the influence of temperature on the capillary and adsorption processes in unsaturated soil. The relationship between the non-isothermal capillary pressure and saturation incorporated the effect of temperature on the immersion enthalpy per unit area, surface tension, and contact angle, as shown by Grant and Salehzadeh [30], where the temperature dependence of the matric suction can be defined as

$$\psi = \psi_{\mathrm{Tr}}\left(\frac{\beta + \mathrm{T}}{\beta_{\mathrm{T_r}} + \mathrm{T_r}}\right) \tag{1}$$

where ψ is the matric suction of the soil [kPa], T is the study temperature [K], ψ_{Tr} is the matric suction at the reference temperature Tr, and β and β_{Tr} are the suction coefficients

[K], depending on the surface tension, immersion enthalpy, and contact angle [30], whose equation can be defined as

$$\beta_{T_r} = \frac{-\Delta h T_r}{-\Delta h + a(\cos\alpha')_{T_r} + b(\cos\alpha')_{T_r} T_r} \tag{2}$$

where a and b are the surface tension parameters at the liquid–air interface, whose values have been confirmed to be estimated as a = 0.11766 Nm^{-1} and b = −0.0001535 $Nm^{-1}K^{-1}$ [31,32], α' is the soil–water contact angle with temperature, cosα' is defined as the k [-], representing the wetting coefficient, and Δh_{Tr} is the enthalpy of immersion per unit area at the reference temperature [J/m^2], whose temperature dependence can be defined as [33]

$$\Delta h = \Delta h_{T_r} \left(\frac{1 - T_r}{1 - T} \right)^{0.38} \tag{3}$$

The enthalpy of immersion per unit area, Δh_{Tr}, was set at −0.285 Jm^{-2} for loam and −0.516 Jm^{-2} for silt at 25 °C [22], representing the thermal change of the solid–gas interface replacing the solid–liquid interface with a liquid. Therefore, the wetting coefficient is expressed as follows [30]:

$$k = \cos\alpha' = \frac{-\Delta h + TC_1}{a + bT} \tag{4}$$

where C_1 is a constant, α' is the soil–water contact angle with temperature, and the value of k represents the sensitivity of the soil to moisture. The angle formed when a liquid comes into contact with a solid surface within soil pores is known as the contact angle. It represents the degree of hydrophilicity of the solid. When the contact angle ranges from 0° to 90°, it is referred to as hydrophilic, indicating a strong affinity for water. Conversely, when the contact angle exceeds 90°, it is considered hydrophobic, indicating a weak affinity for water. To maintain the water-holding mechanism of the soil within the range of the capillary, the soil–water contact angle must be between 0° and 90° [34]. The closer the contact angle is to 0°, the more hydrophilic the soil is and the more sensitive it is to water. Therefore, in order to consider more conservative results in this study, the wetting coefficient at the reference temperature was set to 0.999 for the subsequent analyses.

2.2. Soil Water Characteristic Curve

The soil water characteristic curve (SWCC) can be used to describe the relationship between matric suction and effective saturation of soils, which is an important indicator to investigate the hydraulic behavior of unsaturated soils. Therefore, to obtain a complete SWCC with limited data, several SWCC models have been derived. In this study, three well-known SWCC models [35–37] were selected to investigate the differences between the different models under the influence of environmental temperature changes: Brooks and Corey [35] (referred to as the BC model):

$$\begin{cases} S_e = \frac{\theta - \theta_r}{\theta_s - \theta_r} = \left(\frac{\alpha}{\psi} \right)^n & \psi < \alpha \\ S_e = 1 & \psi \geq \alpha \end{cases} \tag{5}$$

van Genuchten [36] (referred to as the VG model):

$$S_e = \frac{\theta - \theta_r}{\theta_s - \theta_r} = \left\{ 1 + [\alpha\psi]^n \right\}^{-(1-1/n)} \tag{6}$$

Kosugi [37] (referred to as the LN model):

$$S_e = \frac{\theta - \theta_r}{\theta_s - \theta_r} = Q\left[\frac{\psi/\alpha}{n} \right] \tag{7}$$

$$Q(x) = \operatorname{erfc}\left(\frac{x/\sqrt{2}}{2}\right) \tag{8}$$

Kosugi [37] further modified the previously proposed model using natural logarithms and is therefore referred to as the LN model. In the proposed three SWCC models, S_e represents effective saturation [-] and is between 0 and 1, θ is volumetric water content [-], θ_s is saturated water content [-], θ_r is residual water content [-], α is the model parameter related to the inverse of the pressure value of air entry [1/m], and n is the model parameter related to the pore size distribution [-].

The three common SWCC models—BC, VG, and LN—can be extended to non-isothermal conditions using the matric suction temperature dependence theory presented in Section 2.1. The extension of the BC model to non-isothermal conditions is as follows:

$$\begin{cases} S_e = \left(\dfrac{\alpha}{\psi\left(\frac{\beta_{T_r}+T_r}{\beta+T}\right)}\right)^n & \psi < \alpha \\ S_e = 1 & \psi \geq \alpha \end{cases} \tag{9}$$

Similar to the BC model, the non-isothermal expansion equation for the VG model is as follows:

$$S_e = \left\{1 + \left[\alpha\psi\left(\frac{\beta_{T_r} + T_r}{\beta + T}\right)\right]^n\right\}^{-(1-1/n)} \tag{10}$$

And the non-isothermal expansion equation of the LN model is shown below:

$$S_e = Q\left[\frac{\psi\left(\frac{\beta_{T_r}+T_r}{\beta+T}\right)/\alpha}{n}\right] \tag{11}$$

$$Q(x) = \operatorname{erfc}\left(\frac{x/\sqrt{2}}{2}\right) \tag{12}$$

By using the matric suction temperature dependence theory, an extended non-isothermal SWCC model can be obtained, which can be used to show how soil hydraulic properties are affected by temperature changes and to conduct subsequent analysis. We analyze the sensitivity of the parameter a, which is related to the air entry value, and the parameter n, which is related to the pore size distribution, to the temperature change and analyze the differences and limitations between the models.

2.3. Seepage Analysis

This study used the HYDRUS 2D [38] module to evaluate and analyze the seepage processes in unsaturated soils. The HYDRUS 2D module is based on the Richards equation [39], which develops two-dimensional and transient seepage control equations to determine the hydraulic properties of unsaturated soil. In this module, the water movement process in the soil is described based on the equilibrium conditions of gravity, capillary pressure, and infiltration pressure, making the module suitable for studying water infiltration and migration in unsaturated soils. The analytical solution for infiltration in the transient unsaturated layer is as follows:

$$\frac{\partial\,\theta(h)}{\partial\,t} = \nabla \cdot K(h)\nabla\,H + W \tag{13}$$

where θ is the volumetric water content [-], t is the time [T], h is the pressure head or suction head [L], H is the total pressure head [L], W represents the seepage caused by pumping or infiltration [T^{-1}], K(h) is the hydraulic conductivity that varies with the pressure head [LT^{-1}], and $\theta(h)$ is the volumetric water content that varies with the pressure head [-].

The hydraulic conductivity function (HCF) used in this study was proposed by Mualem [40] based on Equation (6) and can be described as follows:

$$K = K_S \cdot (S_e)^l \left\{ 1 - \left[1 - (S_e)^{1/m} \right]^m \right\}^2 \tag{14}$$

where Ks is the hydraulic conductivity coefficient in saturated soils [LT^{-1}], l is the soil pore correlation coefficient [-], generally expressed as 0.5, and m = 1-1/n.

2.4. Slope Stability Analysis

2.4.1. Effective Stress in Unsaturated Soils

Since the development of the effective stress theory by Terzaghi [41], the effective stress concept has been widely applied to solve soil mechanics problems, especially in saturated soil. The effective stress is expressed as follows:

$$\sigma' = \sigma - \mu_w \tag{15}$$

where σ' is the effective stress [$ML^{-1}T^{-2}$], σ is the total stress [$ML^{-1}T^{-2}$], and μ_w is the saturated pore water pressure [$ML^{-1}T^{-2}$]. However, this study focused on shallow slope stability. Shallow slope failure usually occurs in unsaturated layers where the soil structure is relatively loose; therefore, the effective stress theory proposed by Terzaghi is not applicable. Therefore, Bishop [42] proposed the concept of matric suction and effective stress parameters, extending and modifying the traditional theory of effective stress in a new form, as follows:

$$\sigma' = \sigma - \mu_a + \chi\psi \tag{16}$$

where μ_a represents the pore air pressure [$ML^{-1}T^{-2}$], and χ is Bishop's effective stress parameter [-], which is a correlation function of soil water content, usually between 0 and 1. According to this stress model, exploring the correlation between soil water content and surface tension is possible.

However, a limitation of Bishop's model is that it ignores the internal stress between soil particles and the influence of other physical and chemical mechanisms in the soil. Therefore, more theoretical support is required for more accurate results. Lu and Likos [43,44] integrated all possible physical and chemical mechanisms between soil particles. The concept of suction stress was proposed [43]:

$$\sigma' = \sigma - \mu_a + \sigma^s \tag{17}$$

where σ^s is the suction stress [$ML^{-1}T^{-2}$]. Because the physicochemical force between soil particles is a function of the soil water content, effective saturation, or matric suction, the suction stress can be expressed as follows [44]:

$$\sigma^s = f(\theta) = f(S) = f(\psi) = -S_e\psi \tag{18}$$

2.4.2. Local Factor of Safety

This study used the local factor of safety (LFS) developed by Lu et al. [45] to evaluate slope stability. The LFS approach, in contrast to the conventional limit equilibrium method, incorporates the Mohr–Coulomb failure criterion and considers the stress state changes induced by rainfall in order to assess the existing stress conditions at different locations along a slope. By considering the failure process and the effects of rainfall, the LFS method provides a more comprehensive evaluation of the stability of slopes. Unlike the limit equilibrium method, which is limited to a single slice or a whole, the LFS can be estimated for each point to determine the potential location of failure. At each point along the slope, the soil strength in the current stress state can be estimated by determining the intersection of the Mohr–Coulomb failure envelope, expressed as the ratio between the stress potential and current stress, as follows [45]:

$$\mathrm{LFS} = \frac{\tau*}{\tau} = \frac{\cos\varphi}{\sigma_1{}' - \sigma_3{}'}\left[2c + (\sigma_1{}' + \sigma_3{}')\tan\varphi\right] \tag{19}$$

where τ* is the shear strength [$ML^{-1}T^{-2}$], representing the potential stress, τ is the shear stress [$ML^{-1}T^{-2}$], representing the current stress, φ is the friction angle of soils, c is the cohesion of soils, and $\sigma_1{}'$ and $\sigma_3{}'$ represent the maximum and minimum effective stress of soils. The average of the maximum and minimum effective stresses is used as the mean effective stress. The Mohr's circle is shifted to the Mohr's Coulomb failure criterion to obtain the shear stress of the soil when damage occurs. When the effective stress decreases due to the increase in water content of the soil, the Mohr's circle is shifted to the left, the reference point of the strength of the soil for the current stress state can be estimated by the intersection intercept between the Mohr's circle and the Mohr's Coulomb failure criterion, and the coefficient of safety for the points inside the slope is defined as local factor of safety. The local coefficient of safety theory is limited in that it ignores net stresses and suction; however, this method is one of the few that can accurately assess the location of slope failures and the stability of each point. Moreover, there is also literature on the assessment of unsaturated soils [46–49]. Therefore, we believe that this theory can be applied in this study.

Furthermore, by referring to the theory of effective stress and suction stress proposed by Lu and Likos [43] and substituting Equation (17) into Equation (19), the following expression is obtained:

$$\mathrm{LFS} = \frac{\tau*}{\tau} = \frac{\cos\varphi}{\sigma_1 - \sigma_3}\left[2c + (\sigma_1 + \sigma_3 - 2\sigma^s)\tan\varphi\right] \tag{20}$$

Equation (20) can be used to analyze the effect of the LFS on slopes owing to changes in the water content or suction stress. When LFS is below 1, it indicates that the point may be in a state of failure. Conversely, the point is relatively stable when the LFS is greater than 1. This relationship helps explain the distribution of potential failure zones and relatively stable zones along the slope. In addition, the LFS method effectively overcomes the difficulties in traditional slope stability analysis as well as analyzes the influence of stability change at each slope position after rainfall infiltration. Therefore, the LFS method has an important application value in slope stability analysis.

2.4.3. Hydro-Mechanical Coupling Stability Analysis

This study used the finite element analysis models HYDRUS 2D [38] and The Slope Cube Module [50] to analyze the seepage and stress changes in unsaturated soils. The Slope Cube Module enables the analysis of stress conditions in soil slopes based on changes in the soil water content. Applying the theory of LFS evaluates the LFS at various depths on shallow slopes. The hydraulically coupled stability analysis process is illustrated in Figure 1. In the analysis model, initially, the transient unsaturated flow analytical solution (Equation (13)) developed by Šimůnek et al. [38] was employed to calculate the variations in soil water content (θ), matric potential (h), and unit weight (γ) at a given time t. Subsequently, the finite element method (FEM) 2D, as presented by Reddy [51], was utilized to analyze the momentum balance (Equation (21)) of the soil, leading to the determination of the distribution of soil stresses.

$$\nabla \cdot (\sigma) + \gamma(\theta)\mathrm{b} = 0 \tag{21}$$

where σ is the stress tensor in the two-dimensional direction of soils, γ(θ) is the soil unit weight influenced by the water content, and b represents the unit vector of gravity. By considering variations in soil moisture content and matric potential, the distribution of stress fields was estimated, allowing for the determination of changes in suction and effective stresses in the soil. Subsequently, the soil stability was assessed using the LFS theory. Once the aforementioned analysis was completed, the calculations continued for the next time step at t + Δt.

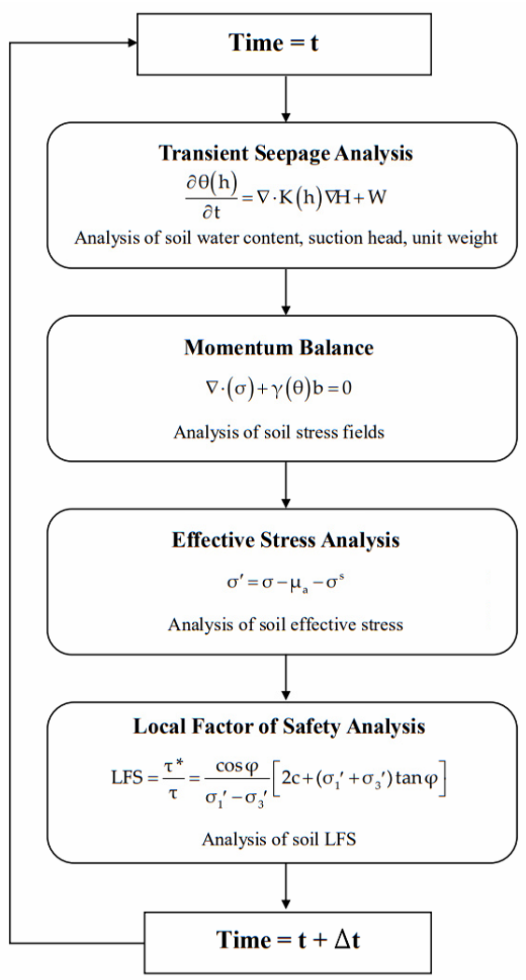

Figure 1. Flow chart of hydro-mechanical coupling stability analysis.

2.5. Research Background Data

2.5.1. Conceptual Model of the Slope

To efficiently quantify the slope failure conditions, a simplified slope model was designed in this study, as illustrated in Figure 2. The slope model was assumed to be a homogeneous slope with a height of 2 m and a slope angle of 30°. The distances from the slope sides to the slope top and the slope angle were 7 and 5 m, respectively, to mitigate the impact of boundary conditions on the seepage process of the slope [52]. The hydrological boundary is the atmospheric boundary at the slope surface, the constant-head boundary at the left and right sides, and the no-flux boundary at the rest of the slope; the force boundary is the free-displacement boundary at the slope surface, the zero-displacement boundary in the x-direction at the left and right sides, and the zero-displacement boundary in the z-direction at the bottom of the slope. Rainfall infiltration boundaries were assigned along segments BC, CD, and DE on the slope surface. According to the Central Weather Bureau guidelines for heavy rainfall, the rainfall intensity was 14.6 mm/h for 24 h. The groundwater level was set up at 6.5 m below the surface, and zero-flux boundaries were imposed at the bottom of the slope above the groundwater level and along the side. An observation profile X-X′ was placed in the middle of the slope. The objective was to observe and analyze the influence of internal soil stresses and stability within a depth of 3 m along the profile during the infiltration process of the rainfall event.

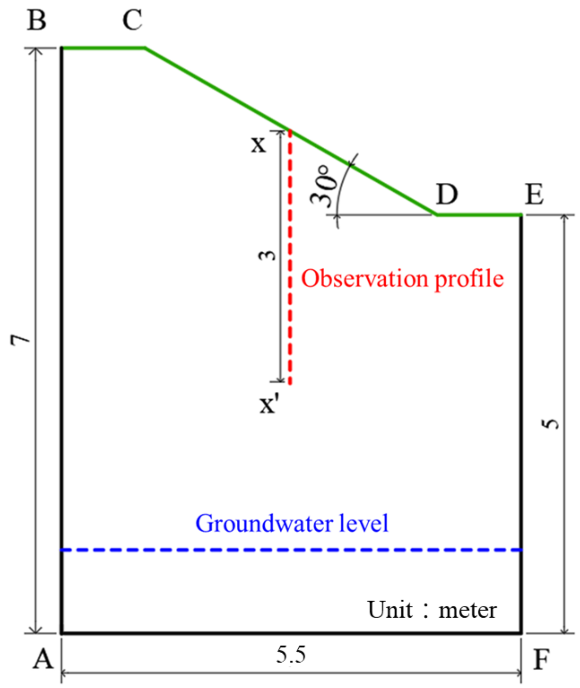

Figure 2. Conception of slope model.

The slope model in this study does not consider vegetation effects. Although vegetation has a soil and water retention effect, it indirectly protects the stability of slopes by performing at least six roles: (1) retains precipitation; (2) reduces runoff velocity and scouring capacity; (3) produces evapotranspiration and lowers the water table; (4) increases soil strength due to the gripping action of the root system but also increases the grain size and porosity of the soil; (5) insulates the soil from the freezing and inflationary effects; and (6) produces a compaction effect on the soil layer. In order to focus on the effect of temperature change on the slope, the effect of vegetation is not considered in this study.

The soil mechanical characteristic parameters were set as listed in Table 1, including the soil specific gravity (G_s), cohesion (c), friction angle (φ), elastic modulus (E), and Poisson's ratio (ν) [53]. The soil hydraulic characteristic parameters included the saturated water content (θ_s), residual water content (θ_r), fitting parameters α and n for the soil water characteristic curve, and unsaturated hydraulic conductivity (K_s) [54], as shown in Table 2. This study investigated two types of standard soil, loam and silt, and employed three SWCC models to fit the hydraulic characteristic parameters for each soil type. The soils used in this study are all based on data from the previous literature. In order to increase the credibility of this study, further experimental validation of the study soils is needed, such as analyzing the main geotechnical properties using the electrical conductivity and permittivity [55] or using physical models to evaluate the process of fluid damage to the soils [56]. This will provide a reference for future research directions.

Table 1. Mechanical properties of soil [53].

	G_s (−)	c (kPa)	φ (°)	E (kPa)	v (−)
Loam	2.65	10	35	15,000	0.3
Silt	2.7	15	30	10,000	0.35

Table 2. Hydraulic properties of soil [54].

BC	θ_s (−)	θ_r (−)	α (kPa^{-1})	n (−)	K_s (m/h)
Loam	0.42	0.033	1.248	0.304	0.036
Silt	0.45	1×10^{-10}	2.847	0.247	0.018
VG	θ_s (−)	θ_r (−)	α (kPa^{-1})	n (−)	K_s (m/h)
Loam	0.43	0.078	0.36	1.56	0.036
Silt	0.46	0.034	0.16	1.37	0.018
LN	θ_s (−)	θ_r (−)	α (kPa^{-1})	n (−)	K_s (m/h)
Loam	0.43	0.098	8.212	1.495	0.036
Silt	0.46	0.072	33.137	2.033	0.018

2.5.2. Study Temperature Criteria

To quantify the impact of different temperature conditions on the stability of shallow slopes, this study was based on the 1 km grid data provided by the Taiwan Climate Change Projection Information and Adaptation Knowledge Platform (TCCIP). The conversion to grid data is based on the estimation of station data [57]. After statistically analyzing the average temperatures in Taiwan from 2016 to 2020, a daily average temperature of 25 °C was set as the reference temperature for this study. Based on statistics from the Central Weather Bureau, Taiwan has observed an average of at least 15 days with temperatures exceeding 35 °C during the summer in recent years. The World Meteorological Organization (WMO) defines temperatures above 35 °C as high temperatures. Therefore, the second study temperature was set at 35 °C, representing daily high temperatures. According to data from the Central Weather Bureau, the current highest recorded temperature in Taiwan is 41.6 °C, which occurred on 21 August 2022 in the Hualien area. Furthermore, the frequency of heat waves and the significant effects of global warming are increasing [5]. Taiwan is also prone to the urban heat island effect, which can increase temperatures by 5 °C during hot days [58]. This indicates that high-temperature conditions are likely to occur more frequently in Taiwan. Therefore, the third study temperature was set at 45 °C, representing extremely high temperatures. By considering the interaction between the three temperature conditions and the two soil types, this study aimed to explore how increasing environmental temperatures affect slope stability. The temperature index set in this study was assumed to be the soil temperature, and rainfall infiltration would not affect the soil temperature; the soil temperature would be considered as a constant value. In this study, it was concluded that water infiltration reduces the soil temperature, which, when assumed to be at a constant high temperature, leads to a reduction in the strength of the soil and allows for more conservative results in the assessment of the potential for landslides.

3. Results and Discussion

3.1. Analysis Results of Soil Water Characteristic Curve

This study initially investigated the effect of temperature on the soil water characteristic curve (SWCC). The results revealed that the SWCC exhibits a general decreasing trend with an increase in temperature. This implies that at a specific effective saturation level, the matric suction decreases with increasing temperature. However, the effect of temperature on the SWCC may differ among different SWCC models. Therefore, we discuss the differences between the three SWCC models and quantify the effect of temperature on the suction value for each model. By comparing the simulation results of the different models, the most suitable model was selected for further study to better understand the variation in SWCC under different temperature conditions.

3.1.1. Results of the BC Model

Using the BC model, when the effective saturation was 0.4, the matric suction of the loam decreased by approximately 18.1% and 29.7% with increased soil temperature from 25 °C to 35 °C and 45 °C, respectively (Figure 3). For silt, the matric suction decreased by approximately 41.9% and 59.1% for the same temperature increments. However, owing to the limitations of BC model equations, they cannot fully capture the hydraulic properties of soils, particularly at low matric suction values. For example, when applying the BC model to silt, the effective saturation of the matric suction below approximately 10 kPa is expressed as 1. Consequently, the model lacks completeness in the low-suction range. Additionally, it is challenging for the BC model to simulate residual saturation because it requires extremely high suction values. These limitations indicate that the BC model may not accurately represent the hydraulic behavior of the soil, particularly in cases involving low matric suction and residual saturation. Therefore, when selecting an appropriate model for simulating soil hydraulic properties, carefully considering the advantages and disadvantages of each model is necessary. The choice of model should be based on specific conditions and requirements to ensure a more accurate representation of the soil moisture behavior.

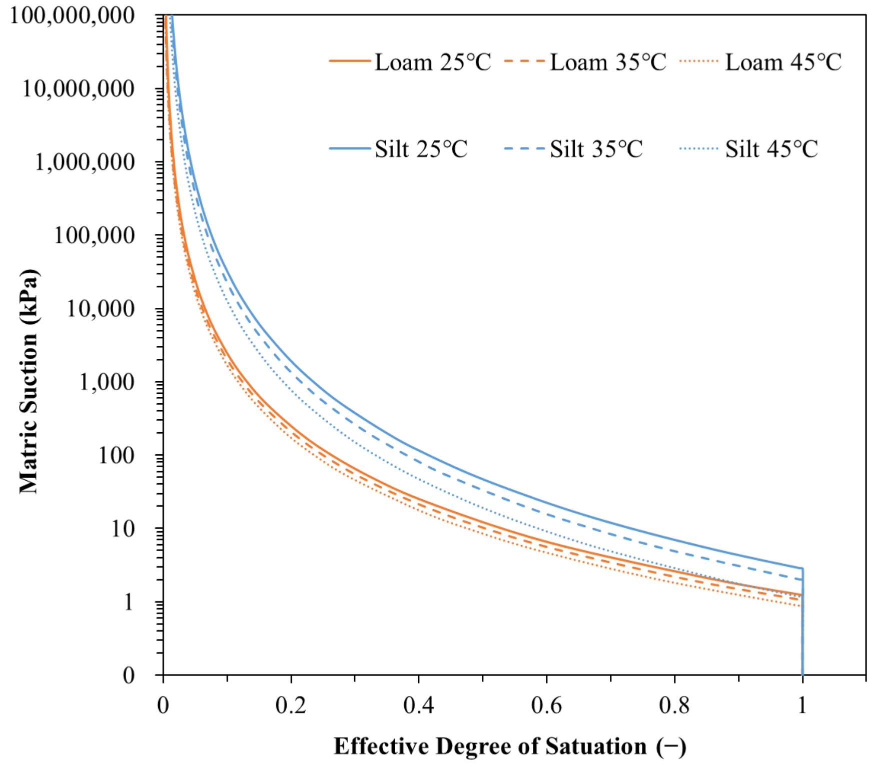

Figure 3. BC model SWCC of different soils at different temperatures.

3.1.2. Results of the VG Model

Using the VG model for simulation, when the soil temperature increased from 25 °C to 35 °C and 45 °C, the matric suction of the loam decreased by approximately 17.7% and 29.8%, respectively. In contrast, the decrease in the matric suction was even greater for silt, with reductions of approximately 42.3% and 59.1%, respectively (Figure 4). These results can be attributed to changes in the surface tension of pore water, enthalpy of immersion, and contact angle as the soil temperature increases, affecting the matric suction in soils. Additionally, the results showed that silt is more sensitive to temperature variations, resulting in a larger decrease in matric suction with increasing temperature. Therefore, when selecting soil models for research, considering the soil characteristics is important to select the most suitable model for simulation and analysis.

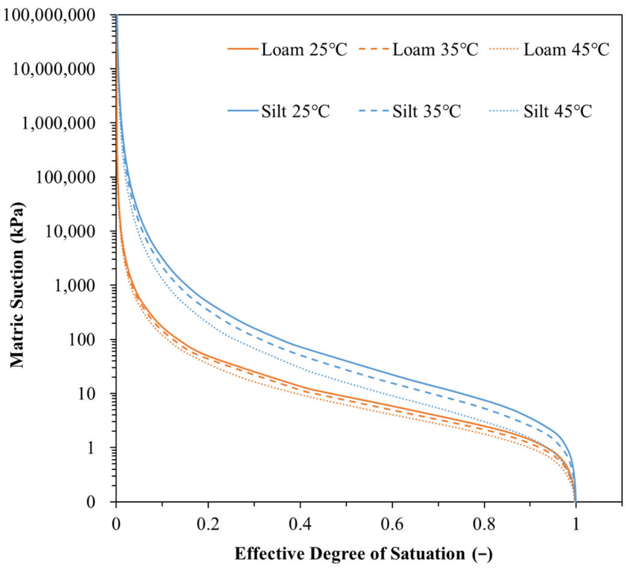

Figure 4. VG model SWCC of different soils at different temperatures.

3.1.3. Results of the LN Model

When using the LN model for simulation, when the soil temperature increased from 25 °C to 35 °C and 45 °C, the matric suction of the loam decreased by approximately 17.5% and 29.6%, respectively, while for the silt, the decrease in matric suction was approximately 42.2% and 59.0%, respectively (Figure 5). The LN model fitting results indicated that the soil tended to easily reach residual saturation. The loam reached residual saturation at approximately 500 kPa of matric suction, while the silt reached residual saturation at approximately 5000 kPa. Therefore, there was very little change in the high-suction range in the effective saturation, and the temperature sensitivity was similar among the models. However, different models exhibited different performance capabilities in the high- and low-suction ranges, particularly in the low-suction range where the effective saturation was below 0.1. The LN model performed better in the low-suction range but was less effective than the VG model in the high-suction range.

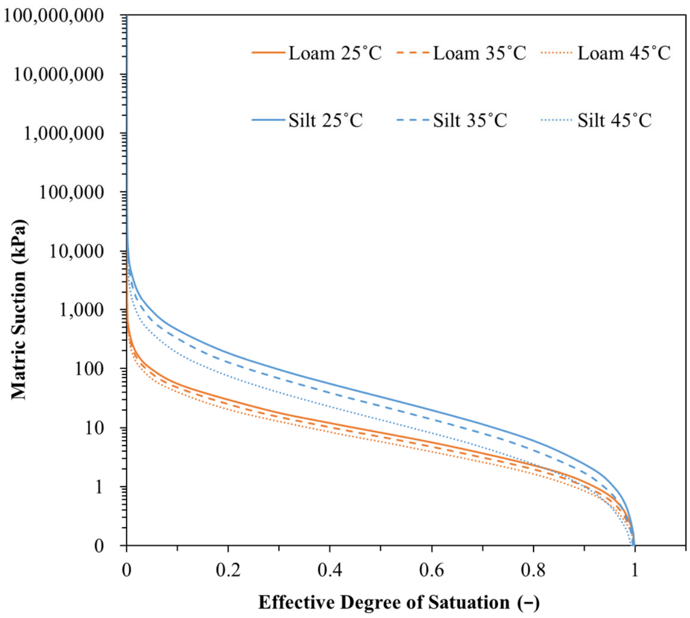

Figure 5. LN model SWCC of different soils at different temperatures.

3.1.4. Summary

An increase in the temperature under certain suction conditions can decrease the effective saturation of the soil. This decrease can be attributed to changes in the surface tension, enthalpy of immersion, and soil–water contact angle. The results demonstrated that the three models showed a similar decreasing trend in the SWCC, and the magnitudes of the decrease caused by the temperature rise were similar. This indicated that these models were equally sensitive to temperature. However, for different soils, the performances of these models in expressing the SWCC were different. Silt with finer particles and a larger surface area led to a stronger water adsorption capacity, causing certain physical quantities related to water to be more susceptible to temperature effects. Consequently, the results revealed that silt exhibited a higher temperature sensitivity than loam. Among the different SWCC models, the BC model lacks completeness in the low-suction range, and the LN model performed better in the low-suction range but was less effective than the VG model in the high-suction range. The analysis showed that the VG model was more likely to capture SWCC variations in the low- and high-suction ranges and performed well for different soils.

3.2. Temperature Sensitivity Analysis of Suction Stress and Effective Stress

To gain a more comprehensive understanding of unsaturated soil mechanics, Lu and Likos [44] proposed a Suction Stress Characteristic Curve (SSCC) based on the traditional concept of stress in soil mechanics and the integration of all possible physical mechanisms occurring between soil particles. The SSCC is used to describe the variation in stress between soil particles under different moisture conditions, and its characteristic suction stress depends on the saturation, water content, or matric suction derived from the SSCC. This concept is similar to the established concepts of SWCC and hydraulic conductivity in unsaturated soils, fully capturing the physical mechanisms between soil particles.

The results of the suction stress characteristic curves (SSCC) presented in Figure 6 demonstrate that the suction stress of the soil is affected by various factors, such as temperature, effective saturation, and matric suction. In different soils, the suction stress exhibited a similar trend; however, the magnitude of changes depended on the degree of capillary adsorption. The results indicated that as the temperature increased, the matric suction and suction stress decreased. This is attributed to changes in the enthalpy of immersion and contact angle caused by temperature variations, subsequently affecting the degree of air entry into the soil suction. However, soils with low permeability exhibited higher variations in suction stress owing to temperature changes at the same matric suction, whereas soils with high permeability exhibited the opposite behavior. Indeed, the effect of lower permeability on capillary adsorption becomes more significant, and different dominant water retention mechanisms exist in different ranges of matric suction. Therefore, soil suction varies under different environmental conditions. In addition, when the suction stress decreased, the shear strength of the soil decreased, which affected the stability of the slope. At a high matric suction, the suction stress appears to approach a constant value, suggesting that an upper limit might exist for typical unsaturated soils.

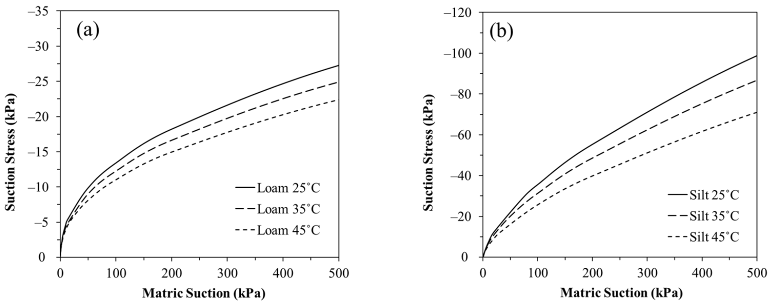

Figure 6. Variation in suction stress with matric suction at different temperatures for (**a**) loam and (**b**) silt.

3.3. Coupled Hydro-Mechanical Framework—Steady State (Hydrostatic Conditions)

3.3.1. Water Content and Suction Stress with Depth

At a steady state under undisturbed conditions, especially in static water conditions, studying variations in soil water content and suction stress with depth is crucial for gaining preliminary insights into soil mechanical properties, with temperature variations playing a significant role. In this study, the stability of shallow slopes is considered, so 3 m is set as an observation depth, which is a complete and clear description of the analytical results of this study. Figure 7a,c illustrate the results of the changes in soil water content with depth, showing that the water content decreased with increasing temperature under stable initial conditions. For example, at a depth of 1 m from the ground surface, the water content of the loam decreased by approximately 4% and 9% when the temperature increased from 25 °C to 35 °C and 45 °C, respectively. Similarly, the water content of the silt decreased by approximately 11% and 30% with the same increase in temperature, respectively. These results suggest that at elevated temperatures, the water content of the soil gradually decreases, potentially affecting the stability of the soil.

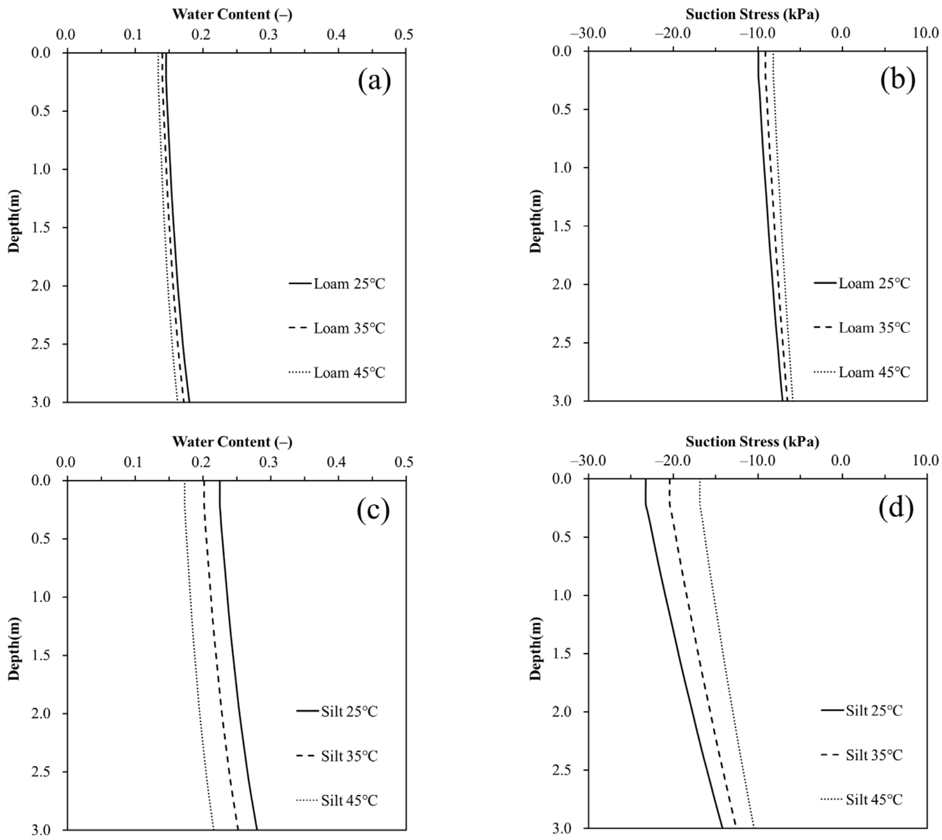

Figure 7. Variation at different temperatures of water content with depth and suction stress with depth.

Figure 7b,d present the results of the changes in suction stress with depth, showing similar trends as the changes in water content. The suction stress decreased with increased temperature. For example, at a depth of 1 m from the surface, the suction stress of the loam decreased by approximately 9% and 21% when the temperature increased from 25 °C to 35 °C and 45 °C, respectively. Similarly, silt suction decreased by approximately 13% and 37% at the same temperature increments. These results indicate that as the environmental temperature increased, the mechanical properties of the soil gradually deteriorated, which negatively affected soil stability. These changes occurred only under still-water conditions, and soil moisture and suction changes became more complex when influenced by external seepage effects. Therefore, when analyzing soil mechanical properties, considering the influence of external conditions on soil behavior is necessary to ensure the accuracy and reliability of the analysis results.

3.3.2. Results of the Local Factor of Safety

Soil suction is an important factor that affects slope stability and is influenced by physical and chemical forces near the contact points of soil particles, such as van der Waals forces. The results of this study indicated that the local safety (LFS) decreased with increasing temperature. Under initial conditions, as the temperature increased, the LFS near the ground surface decreased slightly and then gradually decreased with increasing depth. For example, when the temperature increased from 25 °C to 35 °C and 45 °C, the LFS of the loam decreased by approximately 2% and 4%, respectively, at a depth of 1 m. Similarly, the LFS of silt decreased by approximately 3% and 7% under the same temperature increments, as shown in Figure 8a,c. The suction stress also decreased with increasing temperature. Initially, the LFS remained nearly constant at different suction stresses and temperatures. However, as the temperature increased, the suction stress gradually decreased. For example, at an LFS of 3.0, the suction stress of the loam decreased by approximately 8% and 20% when the temperature increased from 25 °C to 35 °C and 45 °C, respectively. At an LFS of 4.0, the suction stress of the silt decreased by approximately 12% and 32% under the same temperature increments, as shown in Figure 8b,d, respectively. This indicates that lower suction stress can maintain the same slope LFS at higher temperatures.

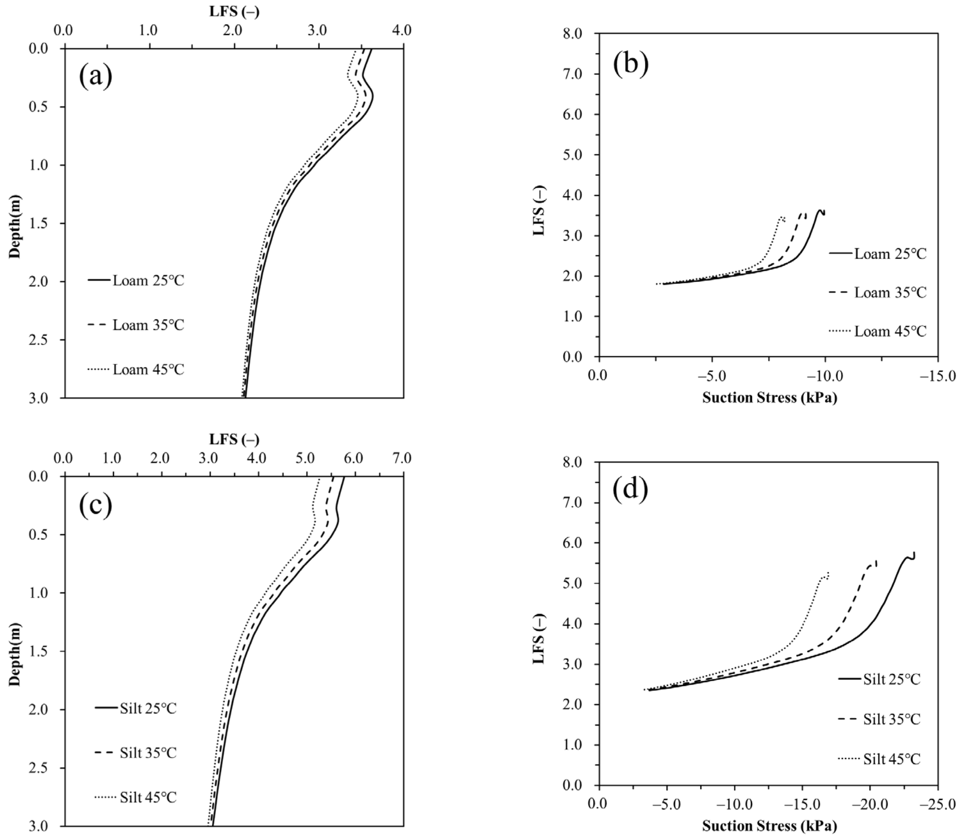

Figure 8. Variation at different temperatures of LFS with depth and LFS with suction stress.

When the local coefficient of safety is greater than one, the slope is considered to be in a stable condition. On the contrary, when the local coefficient of safety is less than one, the slope is in a state of failure. Notably, in the weathering zone at depths below 1 m, the LFS decreased significantly when the temperature increase became more prominent. As the depth increased, the saturation also increased, resulting in a diminishing effect of temperature on the LFS. However, along the critical region of the weak sliding plane, the increased temperature reduced the critical LFS at the slope-monitoring point, possibly resulting in failure earlier than the slope under environmental temperature conditions. Generally, the failure of most slopes occurs in the critical region along the weak sliding plane. Therefore, when evaluating slope stability, it is necessary to carefully consider the influence of temperature on the attraction of soil and the stability of the safety factor.

3.4. Coupled Hydro-Mechanical Framework—Transient Simulation Results

In this study, simulations were performed to evaluate slope stability under uniform rainfall conditions, and the change in profile depth in the middle of the slope was analyzed based on the simulation results. A rainfall intensity of 14.6 mm/h was selected as the basis for this study, and a hydro-mechanical coupled model was employed to simulate rainfall conditions. During a continuous 24 h rainfall event, four time points (t = 0, t = 6, t = 12, t = 24) were selected for instantaneous transient analysis to understand the variations in the mid-slope profile at different time points. To better understand the factors affecting slope stability, this study analyzed the important physical quantities that affect slope stability. By analyzing the physical quantities individually at each point in time, a comprehensive understanding of variations in slope stability can be obtained, thereby improving the predictions of potential geological hazard risks. There are previous studies in the literature on clay slopes subjected to thermal effects [59]. In this study, similar trends as well as results were obtained for different studied soils. However, in order to obtain more accurate results, a further study of the true thermo-hydro-mechanical coupling is required [60].

3.4.1. Results of Water Content with Depth

From the results of moisture content variations, it is evident that rainfall causes a significant infiltration effect. The water content of soils gradually increased with increasing rainfall duration, and the wetting front deepened into the soil profile. Soils in the high-temperature condition had lower water content at all times, and the results showed that increased temperature reduces the water retention capacity of the soil. The soil temperature also has a significant impact on soil infiltration. As the soil temperature increased, the infiltration rate decreased, resulting in slower changes in soil water content. Considering the case of continuous rain for 24 h (t = 24), when the soil moisture reached 0.3, the depth was approximately 1.27 m at the soil temperature of 25 °C, 1.24 m at 35 °C, and only 1.21 m at 45 °C for the loam. Infiltration was more influenced by temperature variation for silt. When the humidity reached 0.3, the depth was approximately 1.58 m at 25 °C, 1.43 m at 35 °C, and only 1.24 m at 45° C (Figure 9). This was attributed to the decrease in the rate of change in soil moisture content with increasing temperature, thus affecting the infiltration depth. In addition, the lower hydraulic conductivity of silt compared to that of loam amplified the effect of temperature variations on infiltration. Increased temperatures effectively change the soil's water retention capacity and infiltration capacity, which in turn changes the soil's suction capacity and stability. A complex relationship exists between soil temperature and water content, which has significant theoretical and practical value for studying soil moisture conditions. The results presented in this study assume full infiltration of rainfall into the soil and therefore do not consider surface runoff from rainfall. In this case, it is possible to focus on the depth-dependent scenario, and the entire slope model does not cause local erosion phenomena during the rainfall process.

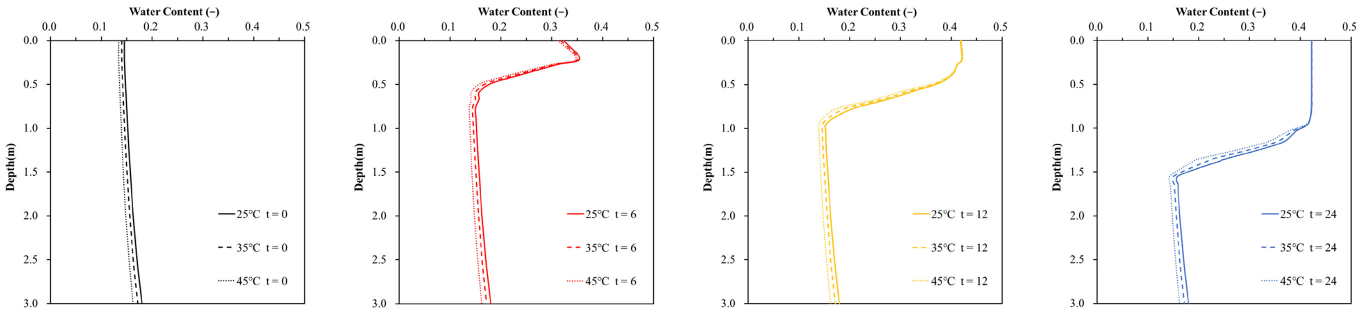

(**a**) loam

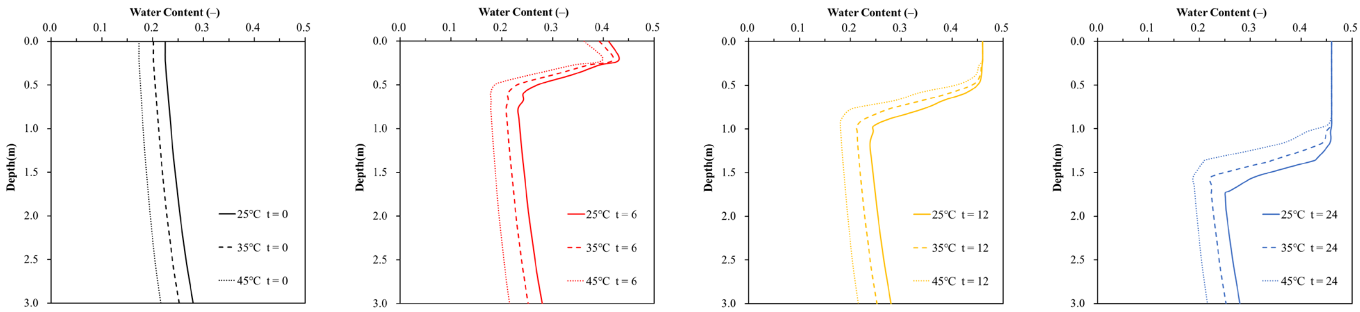

(**b**) silt

Figure 9. Variation in water content with depth at different temperature transients for (**a**) loam and (**b**) silt.

3.4.2. Results of Suction Stress with Depth

During the simulated rainfall process, variations in the soil water content and degree of saturation significantly influenced soil suction. The simulation results (Figure 10) showed that with increasing rainfall duration, the soil water content gradually increased, the degree of saturation gradually increased, and the soil suction stress decreased. The variations in the suction stress depended on the changes in the degree of saturation, thus exhibiting an overall trend similar to that of the water content. Because of infiltration, after 24 h of continuous rainfall, the soil near the surface (at a depth of 1 m) reached saturation, losing suction between the soil particles, resulting in zero suction stress (Figure 10). However, during the 24 h rainfall simulation, there was a marginal difference in suction variation due to changes in soil temperature. This is because the change in temperature causes the differential infiltration rates, and as a result, the changes in suction influence each other. Below the saturation depth range, the change in suction due to temperature change is not significant. The reason for this is that the rate of infiltration caused by temperature rise and the change in suction influence each other, so the effect of temperature change is not significant at this stage. Therefore, there was a significant difference only in the silt after 24 h of rainfall. For example, at a depth of 1.2 m, the suction stresses were 0.85 kPa at 25 °C, 1.96 kPa at 35 °C, and 4.37 kPa at 45 °C. This is because at 45 °C, the water infiltration rate was slower, and thus, saturation was not achieved under the 45 °C condition at this depth. In contrast, at 25 °C and 35 °C, it approached saturation. Therefore, the 45 °C condition exhibited a higher suction stress value in this scenario. As the depth increases, the area unaffected by infiltration remains as it was in the initial state. Relatively low suction values exist for soils at high temperatures due to changes in water content.

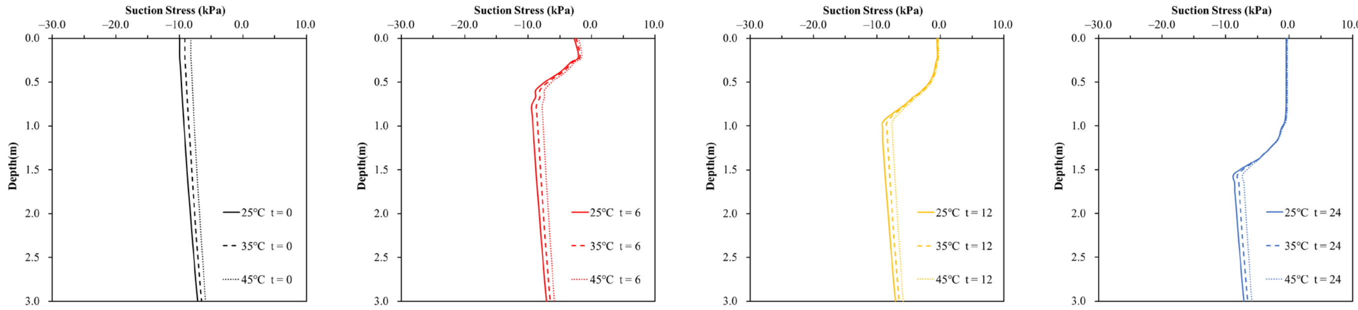

(**a**) loam

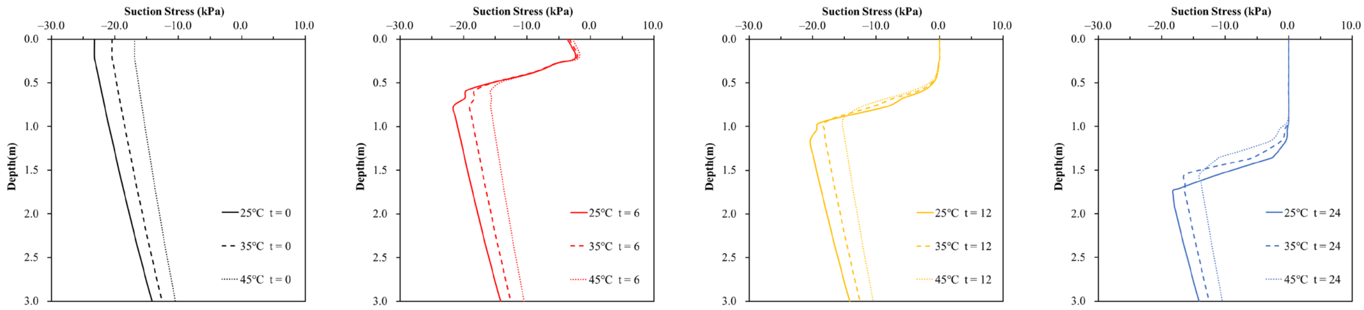

(**b**) silt

Figure 10. Variation in suction stress with depth at different temperature transients for (**a**) loam and (**b**) silt.

3.4.3. Results of the Local Factor of Safety with Depth

According to the theory proposed by Lu et al. [40], the local factor of safety (LFS) depends on the soil cohesion, friction angle, and effective stress. Therefore, the simulation of the LFS results obtained from the hydraulic coupling model was consistent with the effective stress trend. The results indicated that an increase in environmental temperature decreased LFS, implying a reduction in soil strength and a tendency to destabilize the slope. Consistent with the simulations of the mean effective stress, when a rainfall event occurred, this study demonstrated that near-surface soils affected by infiltration exhibited a gradual increase in saturation, accompanied by a corresponding decrease in the LFS. Among the tested conditions, the largest decrease in the LFS was observed at a temperature of 25 °C. In the initial steady state, the soil at 25 °C exhibited a higher LFS than the high-temperature state. However, after rainfall events (t = 6, t = 12, and t = 24), the soil at 25 °C demonstrated a lower LFS (Figure 11). This phenomenon resulted in the appearance of an intersection point in the depth profile of the LFS, which moved towards greater depths as the duration of rainfall increased. The part of the profile above the crossing point exhibited different water retention mechanisms than that at the steady state, which was mainly influenced by capillary action owing to the large amount of water introduced by rainfall. Therefore, a lower temperature corresponded to a lower LFS. This pattern was observed in both loam and silt, indicating that soils with lower relative temperatures exhibited greater enthalpy of immersion and higher contact angles, indicating a higher sensitivity to humidity changes in the presence of water. However, regardless of the effects of rainfall events, high temperatures significantly decrease soil strength, leading to slope instability. In addition, because of the smaller pore sizes of the silt, it exhibited a greater magnitude of variation in the LFS in response to changes in the water content than the loam. Consider the different trends in soil temperature rise before and after rainfall. In practical engineering applications, it is necessary to incorporate the effects of rainfall events to analyze the distribution of water content at various locations on the slope. Then, the effect of soil temperature change should be considered to decide whether high temperature or normal temperature should be considered. This ensures that the assessment of failure potential can be carried out effectively.

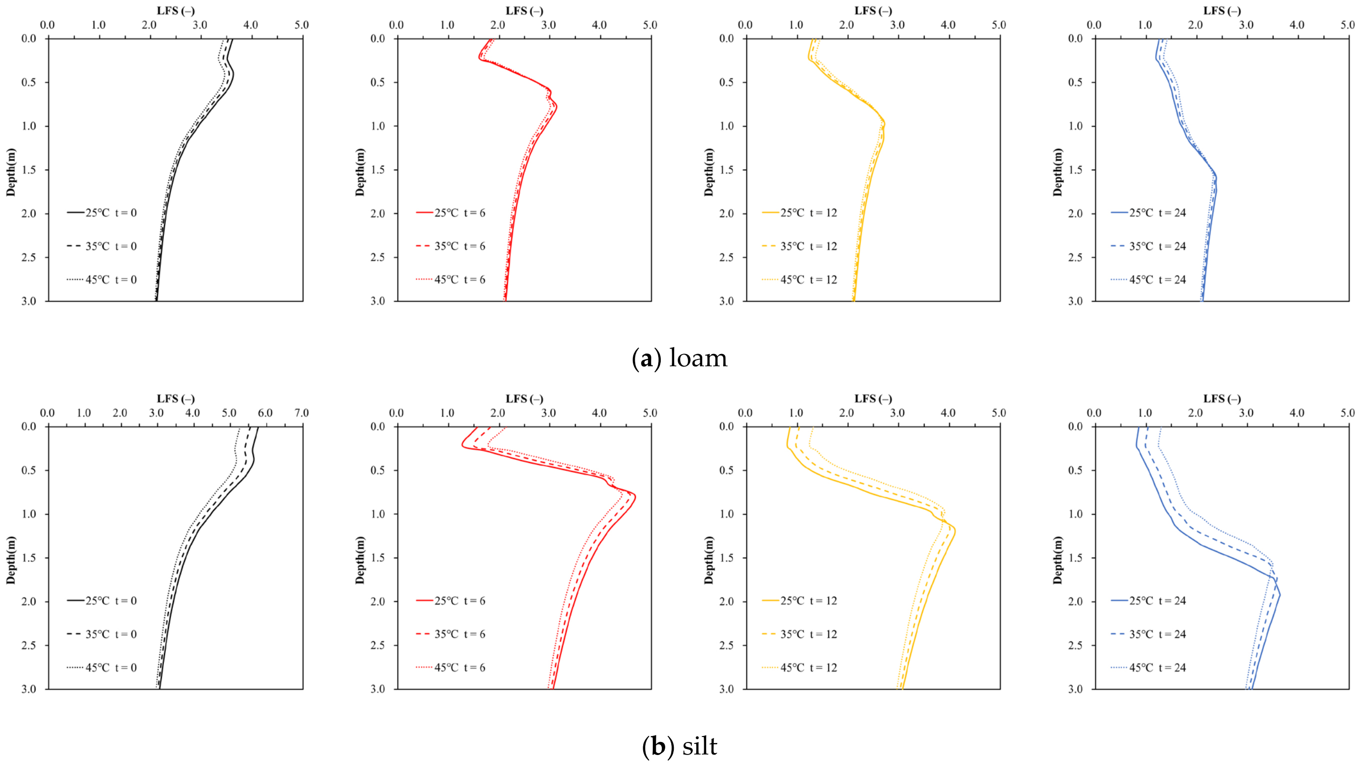

Figure 11. Variation in LFS with depth at different temperature transients for (**a**) loam and (**b**) silt.

4. Conclusions

The change in the temperature state of the soil affects the matric suction of the soil, which is attributed to changes in the surface tension, enthalpy of immersion, and soil–water contact angle. The silt was more sensitive than loam to temperature changes owing to its smaller particle size, resulting in higher water absorption. The results from different SWCC models revealed significant changes with increasing temperature, and the sensitivity to temperature is similar between SWCC models. The study results indicated that the suction stress exhibited a trend similar to the matric suction, where an increase in temperature decreased the absolute value of the matric suction. However, the magnitude of this change depended on the capillary adsorption capacity. As a result, as the matric suction decreases, the shear strength of the soil also decreases, thereby affecting the stability of the slopes.

Analysis of the slope model results revealed that the stability of the soil under rainfall conditions was mainly governed by the change in matric suction and soil permeability, with the degree of change being aggravated by temperature variations. Before rainfall occurred, the soil was affected by existing moisture, and under high temperatures, soil stress and strength decreased, causing the LFS to decrease as the temperature increased. According to the rainfall infiltration process, higher temperatures (35 °C and 45 °C) in saturated soils near the surface lead to a higher LFS, while at normal temperature conditions (25 °C), the LFS is lower. As rainfall and infiltration continued, the soil reached a stress peak at a certain depth, and the LFS reached its maximum. Before and after this peak, the normal and high-temperature conditions were dominated by different water retention mechanisms, exhibiting different stress strength tendencies. Consider the different trends in soil temperature rise before and after rainfall. Soils that are warm before rainfall tend to be unstable. On the contrary, soil in high-temperature conditions after rainfall will be relatively stable. Therefore, in practical engineering applications, it is necessary to take into account the effects of rainfall events and to develop corresponding strategies for slopes with different temperatures. True thermal–hydraulic–mechanical coupling was not considered in this study. More complex equations or other methods are needed to validate the model in this study to improve the credibility of this study.

Author Contributions: S.-R.Y. and R.-E.C. carried out the conception of this work. R.-E.C. and H.-F.Y. performed material acquisition, interpretation, and curation. Y.-S.Y. performed the data visualization and prepared the original draft. H.-F.Y. supervised the writing, reviewing, and editing. All authors have read and agreed to the published version of the manuscript.

Funding: This research received no external funding.

Data Availability Statement: The data that support the findings of this study are available from the corresponding author, H.-F.Y., upon reasonable request.

Conflicts of Interest: The authors declare no conflict of interest.

References

1. Noor, M.; Ismail, T.; Chung, E.-S.; Shahid, S.; Sung, J.H. Uncertainty in Rainfall Intensity Duration Frequency Curves of Peninsular Malaysia under Changing Climate Scenarios. *Water* **2018**, *10*, 1750. [CrossRef]
2. Mori, N.; Takemi, T.; Tachikawa, Y.; Tatano, H.; Shimura, T.; Tanaka, T.; Fujimi, T.; Osakada, Y.; Webb, A.; Nakakita, E. Recent nationwide climate change impact assessments of natural hazards in Japan and East Asia. *Weather Clim. Extrem.* **2021**, *32*, 100309. [CrossRef]
3. Cutter, S.L.; Ismail-Zadeh, A.; Alcántara-Ayala, I.; Altan, O.; Baker, D.N.; Briceño, S.; Gupta, H.; Holloway, A.; Johnston, D.; McBean, G.A. Global risks Pool knowledge to stem losses from disasters. *Nature* **2015**, *522*, 277–279. [CrossRef]
4. Hu, C.; Tam, C.-Y.; Li, X.; Huang, K.; Ren, C.; Fung, K.Y.; Wang, Z. Mega-city development impact on hourly extreme rainfall over the South China Greater Bay Area under near-future climate warming. *Urban Clim.* **2023**, *48*, 101389. [CrossRef]
5. Chiang, F.; Mazdiyasni, O.; AghaKouchak, A. Evidence of anthropogenic impacts on global drought frequency, duration, and intensity. *Nat. Commun.* **2021**, *12*, 2754. [CrossRef] [PubMed]
6. Mukherjee, S.; Mishra, A.K. Increase in Compound Drought and Heatwaves in a Warming World. *Geophys. Res. Lett.* **2021**, *48*, e2020GL090617. [CrossRef]
7. Vardon, P.J. Climatic influence on geotechnical infrastructure: A review. *Environ. Geotech.* **2015**, *2*, 166–174. [CrossRef]
8. Vahedifard, F.; Cao, T.D.; Thota, S.K.; Ghazanfari, E. Nonisothermal Models for Soil–Water Retention Curve. *J. Geotech. Geoenviron. Eng.* **2018**, *144*, 04018061. [CrossRef]
9. Fredlund, D.G.; Rahardjo, H.; Fredlund, M.D. *Unsaturated Soil Mechanics in Engineering Practice*; John Wiley & Sons: Hoboken, NJ, USA, 2012.
10. Rahardjo, H.; Kim, Y.; Satyanaga, A. Role of unsaturated soil mechanics in geotechnical engineering. *Int. J. Geo-Eng.* **2019**, *10*, 8. [CrossRef]
11. Thota, S.K. Temperature effects on unsaturated soils: Constitutive relationships and emerging geotechnical applications. In *Theses and Dissertations*; Mississippi State University: Starkville, MI, USA, 2020; p. 4233.
12. Wang, H.; Chen, R.; Leung, A.K.; Huang, J. Temperature effects on the hydraulic properties of unsaturated rooted soils. *Can. Geotech. J.* **2023**, *60*, 936–945. [CrossRef]
13. Luo, P.; Zhou, M.; Deng, H.; Lyu, J.; Cao, W.; Takara, K.; Nover, D.; Geoffrey Schladow, S. Impact of forest maintenance on water shortages: Hydrologic modeling and effects of climate change. *Sci. Total Environ.* **2018**, *615*, 1355–1363. [CrossRef] [PubMed]
14. Winter, T.C.; Harvey, J.W.; Franke, O.L.; Alley, W.M. Ground Water and Surface Water A Single Resource. In *US Geological Survey*; Diane Publishing: Collingdale, PA, USA, 1998.
15. Sánchez, M.; Arson, C.; Gens, A.; Aponte, F. Analysis of unsaturated materials hydration incorporating the effect of thermo-osmotic flow. *Geomech. Energy Environ.* **2016**, *6*, 101–115. [CrossRef]
16. Nakhaei, M.; Tafreshi, A.M.; Tafreshi, G.M. A New Approach in Comparison and Evaluation of the Overall Accuracy of Six Soil-Water Retention Models Using Statistical Benchmarks and Fuzzy Method. *Eur. Soil Sci.* **2021**, *54*, 716–728. [CrossRef]
17. Zhang, Y.; Zhao, D.; Zheng, Q.; Huang, Y.; Jiang, F.; Wang, M.-K.; Lin, J.; Huang, Y. Evaluating the effects of temperature on soil hydraulic and mechanical properties in the collapsing gully areas of south China. *CATENA* **2022**, *218*, 106549. [CrossRef]
18. Bachmann, J.; Horton, R.; Grant, S.A.; van der Ploeg, R.R. Temperature Dependence of Water Retention Curves for Wettable and Water-Repellent Soils. *Soil Sci. Soc. Am. J.* **2002**, *66*, 44–52. [CrossRef]
19. Grant, S.A.; Bachmann, J. Effect of temperature on capillary pressure. *Environ. Mech. Water Mass Energy Transf. Biosph.* **2002**, *129*, 199–212.
20. Roshani, P.; Sedano, J.Á.I. Incorporating Temperature Effects in Soil-Water Characteristic Curves. *Indian Geotech. J.* **2016**, *46*, 309–318. [CrossRef]
21. Qiao, X.; Ma, S.; Pan, G.; Liu, G. Effects of Temperature Change on the Soil Water Characteristic Curve and a Prediction Model for the Mu Us Bottomland, Northern China. *Water* **2019**, *11*, 1235. [CrossRef]

22. Thota, S.K.; Vahedifard, F. Stability analysis of unsaturated slopes under elevated temperatures. *Eng. Geol.* **2021**, *293*, 106317. [CrossRef]
23. Wu, C. Using the Spatiotemporal Hot Spot Analysis and Multi-Annual Landslide Inventories to Analyze the Evolution and Characteristic of Rainfall-Induced Landslide at the Subwatershed Scale in Taiwan. *Water* **2023**, *15*, 1355. [CrossRef]
24. Hsu, H.-H.; Chou, C.; Wu, Y.; Lu, M.; Chen, C.; Chen, Y.-M. *Climate Change in Taiwan Scientific Report 2011 (Summary)*; National Science Council: Taipei, Taiwan, 2011; 67p.
25. Tung, Y.-S.; Chen, C.-T.; Min, S.-K.; Lin, L.-Y. Evaluating Extreme Rainfall Changes over Taiwan Using a Standardized Index. *Terr. Atmos. Ocean. Sci.* **2016**, *27*, 705–715. [CrossRef]
26. Henny, L.; Thorncroft, C.; Hsu, H.-H.; Bosart, L. Extreme Rainfall in Taiwan: Seasonal Statistics and Trends. *J. Clim.* **2021**, *34*, 4711–4731. [CrossRef]
27. Hsu, H.H.; Chen, C.T. Observed and projected climate change in Taiwan. *Meteorol. Atmos. Phys.* **2002**, *79*, 87–104. [CrossRef]
28. Kueh, M.T.; Lin, C.Y.; Chuang, Y.J.; Sheng, Y.F.; Chien, Y.Y. Climate variability of heat waves and their associated diurnal temperature range variations in Taiwan. *Environ. Res. Lett.* **2017**, *12*, 074017. [CrossRef]
29. Chen, C.-C.; Wang, Y.-R.; Wang, Y.-C.; Lin, S.-L.; Chen, C.-T.; Lu, M.-M.; Guo, Y.-L.L. Projection of future temperature extremes, related mortality, and adaptation due to climate and population changes in Taiwan. *Sci. Total Environ.* **2021**, *760*, 143373. [PubMed]
30. Grant, S.A.; Salehzadeh, A. Calculation of Temperature Effects on Wetting Coefficients of Porous Solids and Their Capillary Pressure Functions. *Water Resour. Res.* **1996**, *32*, 261–270.
31. Dorsey, N.E. *Properties of Ordinary Water-Substance in All Its Phases: Water-Vapor Water and All the Ices*; Reinhold: New York, NY, USA, 1940.
32. Haar, L.; Gallagher, J.S.; Kell, G.S. *NBS/NRC Steam Tables Thermodynamic and Transport Properties and Computer Programs for Vapor and Liquid States of Water in SI Units*; Hemisphere Pub.: Washington, DC, USA, 1984.
33. Watson, K.M. Thermodynamics of the Liquid State. *Ind. & Eng. Chem.* **1943**, *35*, 398–406.
34. Song, J.W.; Fan, L.W. Temperature dependence of the contact angle of water: A review of research progress, theoretical understanding, and implications for boiling heat transfer. *Adv. Colloid Interface Sci.* **2021**, *288*, 102339.
35. Brooks, R.H.; Corey, A.T. Hydraulic Properties of Porous Media and Their Relation to Drainage Design. *Trans. ASABE* **1964**, *7*, 26–28.
36. Van Genuchten, M.T. A Closed-form Equation for Predicting the Hydraulic Conductivity of Unsaturated Soils. *Soil Sci. Soc. Am. J.* **1980**, *44*, 892–898. [CrossRef]
37. Kosugi, K.I. Lognormal Distribution Model for Unsaturated Soil Hydraulic Properties. *Water Resour. Res.* **1996**, *32*, 2697–2703. [CrossRef]
38. Šimůnek, J.; van Genuchten, M.T.; Šejna, M. Development and Applications of the HYDRUS and STANMOD Software Packages and Related Codes. *Vadose Zone J.* **2008**, *7*, 587–600. [CrossRef]
39. Richards, L.A. Capillary conduction of liquids through porous mediums. *Physics* **1931**, *1*, 318–333. [CrossRef]
40. Mualem, Y. A new model for predicting the hydraulic conductivity of unsaturated porous media. *Water Resour. Res.* **1976**, *12*, 513–522.
41. Terzaghi, K. *Theoretical Soil Mechanics*; Wiley: New York, NY, USA, 1943.
42. Bishop, A.W. The Principle of Effective Stress. *Tek. Ukebl.* **1959**, *39*, 859–863.
43. Lu, N.; Likos, W.J. *Unsaturated Soil Mechanics*; John Wiley & Sons, Inc.: Hoboken, NJ, USA, 2004; pp. 30–45.
44. Lu, N.; Likos, W.J. Suction Stress Characteristic Curve for Unsaturated Soil. *J. Geotech. Geoenviron. Eng.* **2006**, *132*, 131–142. [CrossRef]
45. Lu, N.; Şener-Kaya, B.; Wayllace, A.; Godt, J.W. Analysis of rainfall-induced slope instability using a field of local factor of safety. *Water Resour. Res.* **2012**, *48*, 9. [CrossRef]
46. Erdağ, A.; Sinan Işık, N. Effect of rainfall ıntensity on the stability of unsaturated slopes of silty clay soils of Kazan, Ankara, Turkey. *Arab. J. Geosci.* **2022**, *15*, 894. [CrossRef]
47. Que, Y.; Ding, H.; Jiang, Z.; Chen, X.; Li, S.; Leung, A.K. Non-equilibrium seepage characteristics and stability analysis of macroporous soil slope under water level changes. *Arab. J. Geosci.* **2022**, *15*, 943. [CrossRef]
48. Yang, Y.-S.; Yeh, H.-F.; Ke, C.-C.; Chen, N.-C.; Chang, K.-C. Assessment of probability of failure on rainfall-induced shallow landslides at slope scale using a physical-based model and fuzzy point estimate method. *Front. Earth Sci.* **2022**, *10*, 957506. [CrossRef]
49. Yang, T.; Rao, Y.; Ma, N.; Feng, J.; Feng, H.; Wang, H. A new method for defining the local factor of safety based on displacement isosurfaces to assess slope stability. *Eng. Geol.* **2022**, *300*, 106587. [CrossRef]
50. Lu, N.; Wayllace, A.; Chen, P. The Slope Stress and Stability (Slope Cube) Module for HYDRUS (3D): Simulating Slope Stress and Stability in Variably-Saturated Soils. In *Hydrus Software Series 3.02.0290, PC-Progress*; Soil Water Retention, LLC: Madison, WI, USA, 2019.
51. Reddy, J.N. *Introduction to the Finite Element Method*, 4th ed.; McGraw-Hill Education: New York, NY, USA, 2019.
52. Kristo, C.; Rahardjo, H.; Satyanaga, A. Effect of hysteresis on the stability of residual soil slope. *Int. Soil Water Conserv. Res.* **2019**, *7*, 226–238. [CrossRef]
53. MnDOT Pavement Design Manual. *Minnesota Department of Transportation*; Minnesota Department of Transportation: St. Paul, MN, USA, 2007.
54. Carsel, R.F.; Parrish, R.S. Developing joint probability distributions of soil water retention characteristics. *Water Resour. Res.* **1988**, *24*, 755–769.

55. Vergnano, A.; Oggeri, C.; Godio, A. Geophysical–geotechnical methodology for assessing the spatial distribution of glaciolacustrine sediments: The case history of Lake Seracchi. *Earth Surf. Process. Landf.* **2023**, *48*, 1374–1397. [CrossRef]
56. Bai, H.-l.; Feng, W.-k.; Li, S.-q.; Ye, L.-z.; Wu, Z.-t.; Hu, R.; Dai, H.-c.; Hu, Y.-p.; Yi, X.-y.; Deng, P.-c. Flow-slide characteristics and failure mechanism of shallow landslides in granite residual soil under heavy rainfall. *J. Mt. Sci.* **2022**, *19*, 1541–1557.
57. Lin, L.-Y.; Lin, C.-T.; Chen, Y.-M.; Cheng, C.-T.; Li, H.-C.; Chen, W.-B. The Taiwan Climate Change Projection Information and Adaptation Knowledge Platform: A Decade of Climate Research. *Water* **2022**, *14*, 358. [CrossRef]
58. Hsu, C.-Y.; Ng, U.-C.; Chen, C.-Y.; Chen, Y.-C.; Chen, M.-J.; Chen, N.-T.; Lung, S.-C.C.; Su, H.-J.; Wu, C.-D. New land use regression model to estimate atmospheric temperature and heat island intensity in Taiwan. *Theor. Appl. Climatol.* **2020**, *141*, 1451–1459.
59. Liu, Z.; Wang, X.; Yin, Y.; Li, J.; Shao, G. Stability analysis of an unsaturated clay slope based on the coupled effect of temperature and saturation. *Q. J. Eng. Geol. Hydrogeol.* **2022**, *55*, qjegh2021-009. [CrossRef]
60. Scaringi, G.; Loche, M. A thermo-hydro-mechanical approach to soil slope stability under climate change. *Geomorphology* **2022**, *401*, 108108.